Hindawi Publishing Corporation
Advances in Acoustics and Vibration
Volume 2012, Article ID 316761, 13 pages
doi:10.1155/2012/316761

Research Article

Gas Turbine Blade Damper Optimization Methodology

R. K. Giridhar,[1] P. V. Ramaiah,[2] G. Krishnaiah,[2] and S. G. Barad[1]

[1] *Vibration Engineering Group, Gas Turbine Research Establishment, CV Raman Nagar, Bangalore 560093, India*
[2] *Mechanical Engineering Department, Sri Venkateswara University, Tirupati 517502, India*

Correspondence should be addressed to R. K. Giridhar, giridhardrdo@gmail.com

Received 11 May 2011; Revised 2 January 2012; Accepted 10 January 2012

Academic Editor: Benjamin Soenarko

The friction damping concept is widely used to reduce resonance stresses in gas turbines. A friction damper has been designed for high pressure turbine stage of a turbojet engine. The objective of this work is to find out effectiveness of the damper while minimizing resonant stresses for sixth and ninth engine order excitation of first flexure mode. This paper presents a methodology that combines three essential phases of friction damping optimization in turbo-machinery. The first phase is to develop an analytical model of blade damper system. The second phase is experimentation and model tuning necessary for response studies while the third phase is evaluating damper performance. The reduced model of blade is developed corresponding to the mode under investigation incorporating the friction damper then the simulations were carried out to arrive at an optimum design point of the damper. Bench tests were carried out in two phases. Phase-1 deals with characterization of the blade dynamically and the phase-2 deals with finding optimal normal load at which the blade resonating response is minimal for a given excitation. The test results are discussed, and are corroborated with simulated results, are in good agreement.

1. Introduction

The friction damping concept is widely applied in turbomachinery applications, especially at hot end parts, to reduce resonance stresses. A typical application of this in gas turbines. They are popularly called as "friction damper," "cottage-roof damper" or "under platform damper." This damper is loaded by centrifugal force against the underside of the platforms of two adjacent blades. The main design criterion for such devices is to determine the optimum damper configuration or the damper mass or both in order to reduce the dynamic stresses to maximum possible extent. For example, if the damper mass is too small for a given configuration, the friction force will not be large enough to dissipate sufficient energy. On the other hand, if the damper mass is too large, it will get into "stick" condition, thereby limiting the relative motion across the interface and hence the amount of energy dissipation. In both cases, the friction damper will be inefficient, and between these two extremes there exists an optima.

A good review of the friction damping concept in turbomachinery applications is given by Griffin [1]. Theoretical analysis and the optimization of this simple device is difficult because of marked nonlinearity and assumptions about the contact characteristics and damper behavior. Several friction damper models and analysis methods have been proposed in past. The simplest and most commonly used model reported in the literature is a macroslip contact model [2–4]. There are also several micro-slip friction models reported which are more appropriate in case of high normal loads [5–10]. The macroslip model under this high normal load shows damper in lockup condition.

Although significant advances are made in theoretical modeling of friction dampers and analysis methods, turbomachinary manufacturers still rely on previous experience and empirical data rather than computer-based predictions alone for friction damper optimization. This has been mainly due to the oversimplification introduced in the models regarding the basic contact behavior and/or damper geometry and the inability to analyze representative-size models due to excessive computational cost [4].

The latest and most advanced contact models make use of three parameters to characterize the contact behavior, namely, friction coefficient, tangential contact stiffness and

normal contact stiffness [11–13]. Szwedowicz et al. [13] investigated numerically and experimentally the performance of a thin-walled damper mounted under the platform of two rotating free-standing high-pressure turbine blades. Characterization of friction contact of nonspherical contact geometries obeying the Coulomb friction law with constant friction coefficient and constant normal load is proposed by [14]. Firrone et al. [15] undertook forced response studies of bladed disc under platform damper considering both static and dynamic displacements.

This paper presents a methodology which combines three essential phases of friction damping optimization in turbomachinery. The first phase is to develop an analytical model of the blade damper system. The second phase is experimentation and model tuning necessary for response studies; while the third phase is evaluating damper performance and arriving at optimal damper design point. Figure 1 gives the flow chart of complete design methodology. In the present work, we are limiting our discussions to static bench test and using this data along with results from analytical studies, studying the damper performance, and then arriving at an optimal damper design.

2. Development of a Mathematical Model

The development of a mathematical model for a blade damper involves following steps:

(1) estimation of eigenvalues and establishment of stress distribution for a specific mode of interest;

(2) development of a friction model;

(3) conducting response studies using reduced model.

2.1. Eigenvalue Estimation and Response Studies. The objective of this phase is to obtain modal characteristics of the blade and stress distribution along the aerofoil for a particular mode of interest along with estimation of nondimensional parameters. Figure 2 presents a finite element 3D model of a turbine blade, with boundary condition in the form of root fixation. The blade material is transversally anisotropic with minimal rigidity axis directed along the blade radius.

Analysis is performed for natural frequencies, distribution of stresses, deformations, and displacements for first six modes. Table 1 gives the various frequencies estimated for various conditions; all the frequencies are normalized with respect to first flexural mode of the blade.

The optimization study is undertaken for the first flexure mode of the blade alone; therefore, we are limiting our discussions to this only. Figures 3 and 4 show the 1st flexural mode of the blade and corresponding stress distribution, respectively. The values corroborate well with the experimental results given in Table 2. The maximum stress is located near the fillet area close to the first lobe of the fir tree.

With the input drawn from above data, the following coefficients are estimated in order to establish the damper design parameters. These are

(1) all the natural frequencies normalized with respect to 1st flexural mode of the blade;

(2) ratio of maximum stresses in the attachment to stresses in aerofoil root, $k_{\sigma\sigma} = 1.86$;

(3) ratio of maximum total displacement to stresses in aerofoil, $k_{u\sigma} = 2.12e^{-3}$ mm^3/N;

(4) ratio of displacement (circumferential direction) at contact location of damping insert to maximum displacement of blade aerofoil, $k_{uu} = 0.07$;

(5) ratio of tip displacement to load amplitude, $k_{uP} = 0.026$.

Further results from the 3D model calculations were used for identifying strain gauge locations for experimental studies.

2.2. Friction Model. The friction interface between the blade root and the damper insert under investigation has a rectangular shape. It is thus appropriate to use a friction interface model that has a rectangular contact surface, such as the model by [5, 9], further the normal load distribution is assumed to be constant over the interface. The model that is used in this paper, shown in Figure 5, is derived from both Menq et al's [5] and the Csaba's one-bar model [9]. The normal load on the damper is assumed as uniform. Further displacement and force is represented in terms of slip length, this feature is derived from Csaba's work [8].

The interface is considered as a rectangular cross-section and modeled as a bar pressed against a rigid surface with a normal load $q(x)$, and the force of P is applied at the end of the bar. The bar has a modulus of elasticity E and area of cross-section A. L, is the length of the bar. The coefficient of friction μ is assumed as constant across the interface and independent of motion of the bar. The normal load across the interface is assumed uniform and constant.

The assumed function of normal load is $q(x) = q_0$, and the total normal load is found by integrating the normal load function over the length of the bar:

$$N = \int_0^L q(x)dx. \tag{1}$$

In the present work, the derivation of displacement function is not presented, but relevant equations as and when required are given.

(1) *Governing Equation.* It is assumed that the bar deforms elastically and the friction is governed by Coulomb's law at each contact point. By applying the load P at the one end of the bar, the onset of slip takes place. Further by increase in amplitude of "P" propagates of slip zone until a gross level slip is achieved. In order to formulate the equation, this bar length is divided into two parts, sliding and not sliding, as shown in Figure 6. The sliding length, that is, the slip zone length is given by "δ" and its maximum value is given by δ_a, corresponding to max force P_a. The friction force is defined by F, and its direction depends on the direction of resultant strain. The displacement at the end of bar is defined as "u."

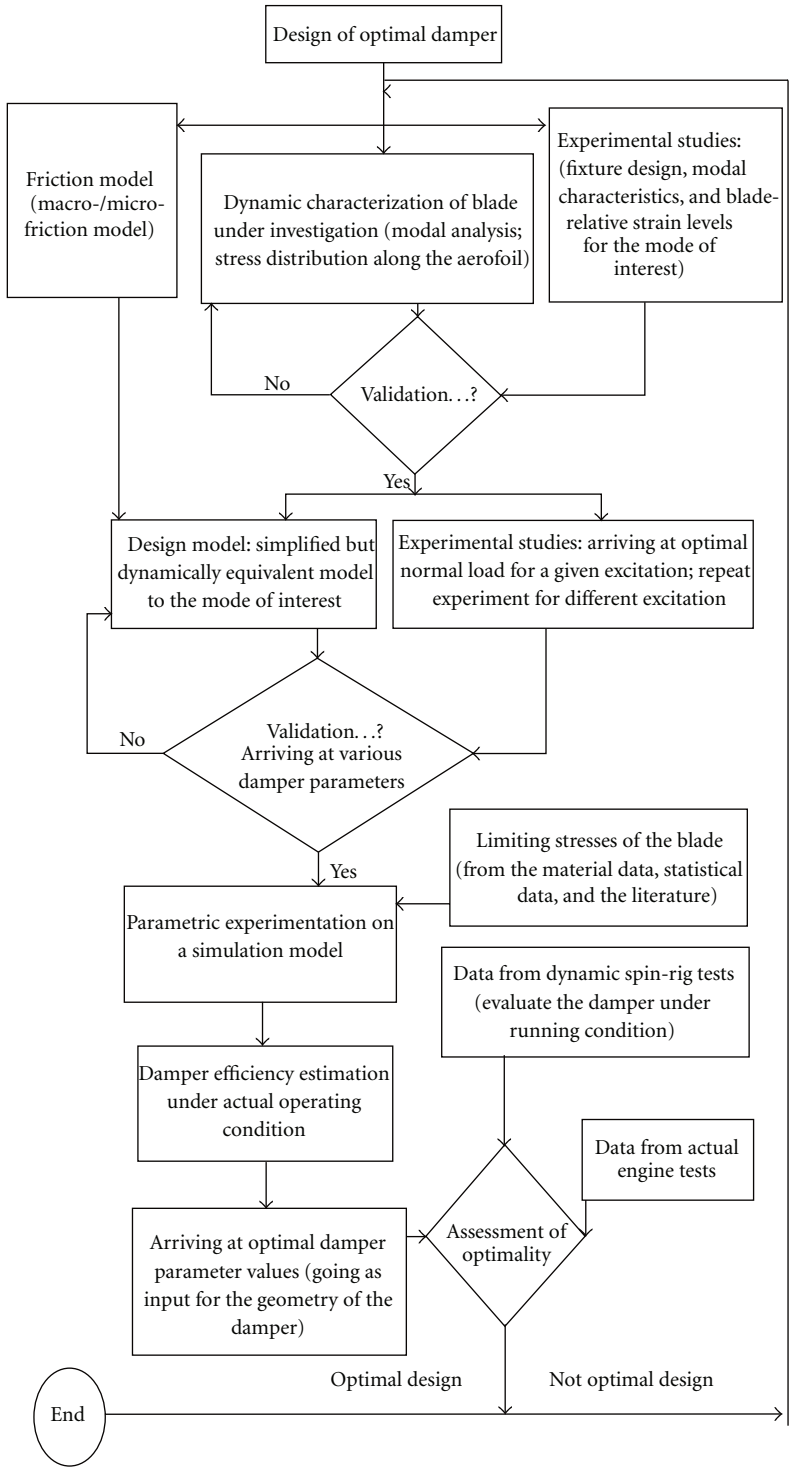

Figure 1: The flow chart indicating the damper design methodology.

The procedure for derivation of displacement function and the force function is followed from [8].

The force is considered as monotonic between its peak values, with amplitude P_a, then the analysis may be divided into three parts with the bar initially at rest [8]:

P is increased from 0 to P_a;

P is decreased from P_a to $-P_a$;

P is increased from $-P_a$ to P_a.

(2) *Formulation of Initial Loading Relations.* The Coulomb's friction law says

$$F = \mu q(x). \tag{2}$$

Table 1: Estimated eigenvalues for various conditions normalized with 1st natural frequency at room temperature.

Mode number and frequency (Hz)				Simulated condition/constraints
1	2	3	4	
f1	1.74f1	2.26f1	3.06f1	Nonrotating blade at room temperature
1.008f1	1.755f1	2.27f1	3.08f1	Rotating at 50% RPM at room temperature
1.056f1	1.79f1	2.30f1	3.16f1	Rotating at 100% RPM at room temperature
0.95f1	1.61f1	2.06f1	2.85f1	Rotating at 100% RPM at 800°C average blade temperature

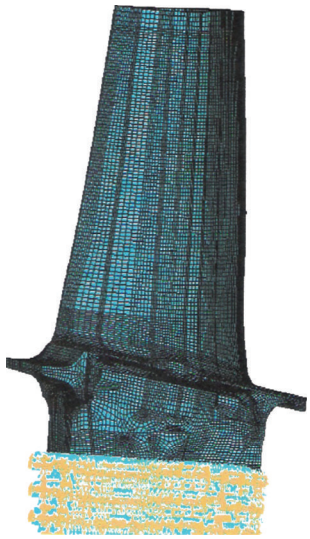

Figure 2: Finite element model of the blade.

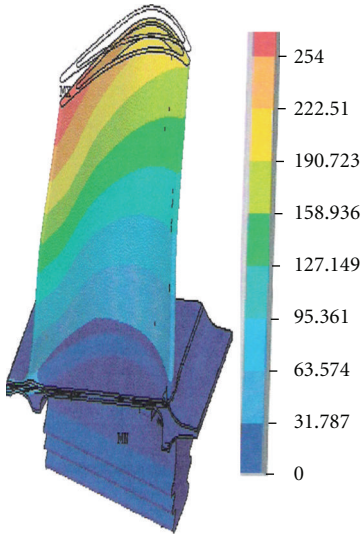

Figure 3: Mode shape for the 1st flexure mode of the blade.

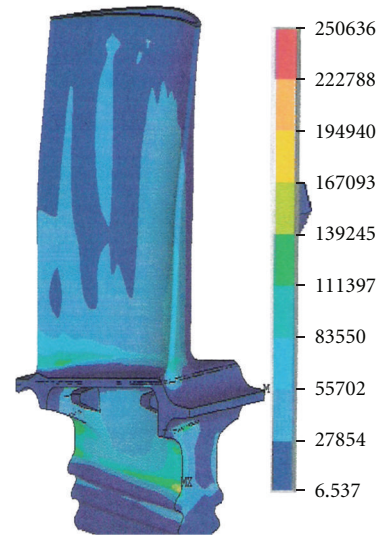

Figure 4: Distribution of equivalent blade stresses at the 1st vibration mode.

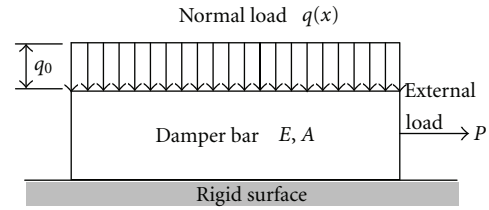

Figure 5: Microslip model for friction interface.

Table 2: Comparison of estimated eigenvalues with experimentally measured values.

Mode number	Estimated values	Experimental values
1	f1	1.01f1
2	1.74f1	1.76f1
3	2.26f1	2.27f1
4	3.06f1	3.12f1

The various forces acting on a small element of length dx of the sliding zone are given in Figure 7. The direction of "F" depends on whether force "P" is increasing or decreasing with respect to "x."

Equilibrium of forces yields

$$F dx + P + \frac{dP}{dx} dx = P. \tag{3}$$

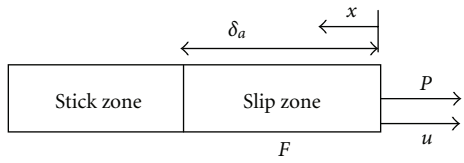

Figure 6: Slip and Stick zones, when the bar is subjected to initial loading.

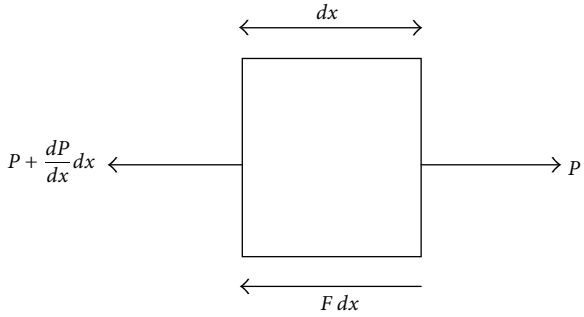

Figure 7: Forces acting on a small element.

The strain in bar is

$$\varepsilon = -\frac{du}{dx}. \tag{4}$$

The tensile force in the bar is defined as

$$P = -EA\left.\frac{du}{dx}\right|_{x=0}. \tag{5}$$

Substituting (5) in (3) we get

$$Fdx - EA\frac{d^2u}{d^2x} = 0, \tag{6}$$

where du/dx is the strain in the bar. The displacement "u" is found by double integrating over the slip zone length using the following boundary conditions [8]:

$$\begin{aligned} &x = 0, \\ &P = -EA\frac{du}{dx}, \qquad x = \delta,\ u = 0. \end{aligned} \tag{7}$$

Therefore, the displacement as a function of force is

$$u(x,P) = P\frac{(x-\delta)}{EA} + \mu q_0\frac{(\delta^2 - x^2)}{2EA}. \tag{8}$$

The force at the bar end can be expressed as a function of the slip length. This is done by integrating the friction force over the slip length [8]:

$$P(\delta) = \int_0^\delta F_x dx = \mu q_0 \delta. \tag{9}$$

The displacement in terms of slip length is given by substituting (9) in (8):

$$\begin{aligned} u(\delta,x) &= \mu q_0\delta\frac{(x-\delta)}{EA} + \mu q_0\frac{(\delta^2 - x^2)}{2EA}, \\ u(\delta,x) &= \mu q_0\frac{(\delta - x)^2}{2EA}. \end{aligned} \tag{10}$$

After having the force and displacement as functions of slip length. Applying "P_{amp}" will give amplitude slip length "δ_a". The force amplitude function is defined by

$$P(\delta_a) = \mu q_0 \delta_a. \tag{11}$$

And the displacement function is given as

$$u(\delta_a) = \frac{\mu q_0 \delta_a^2}{2EA}. \tag{12}$$

(3) *Load Decreasing Relations.* The section of the bar that was slipping is stretched after an initial loading of $P = P_{\text{amp}}$. This is given as broken line in Figure 8. The bar is divided into three zones shown in Figure 8, as given in [8]. Zone "Z," where tension is changing in to compression will extend, as the force is decreasing from P_{amp} to $-P_{\text{amp}}$. The length of the compression zone length is denoted as δ_d. Zone Z will increase, and zone Y will decrease as P is decreasing, this will continue till $P = -P_{\text{amp}}$. Zone Y is then eliminated, and δ_d equals δ_a.

The friction force direction depends on the sign of dP on that part. The various forces acting on a small element of length dx of zone "Z" is given in Figure 9. The differential equation for this is

$$Fdx + EA\frac{d^2u}{d^2x} = 0. \tag{13}$$

The boundary conditions are found by equilibrium of forces at the bar end, and with a condition that u_a, and u_d must be of the same value, where zone Y and Z are connected. These boundary conditions are, as given in [8]:

$$\begin{aligned} &x = 0, \\ &P = -EA\frac{du_d}{dx}, \qquad x = \delta_d,\ u_d(\delta_a,\delta_d) = u(\delta_a,\delta_d). \end{aligned} \tag{14}$$

Solving (13) by substituting (14) yields u_d. The displacement of the bar end will be a function of δ_a and δ_d.

The displacement function is given as

$$u_d(\delta_a,\delta_d) = \frac{\mu q_0\left(\delta_a^2 - \delta_d^2\right)}{2EA}. \tag{15}$$

The slip length δ_d is found by equilibrium of forces for the compressed region Z. By equilibrium of forces as shown in Figure 10 and solving one gets the force in terms of slip length. This is given by

$$P_d(\delta_a,\delta_d) = \mu q_0(\delta_a - 2\delta_d), \tag{16}$$

where δ_d is the slip length, when load is decreasing from P_{amp} to $-P_{\text{amp}}$.

(4) *Reloading Relations.* This is exactly opposite situation to the one in previous section. Zone Z, where tension will be seen in place of compression, will increase and extend as the force is increasing from $-P_{\text{amp}}$ to P_{amp}. The strain in the bar when force P is increasing is shown as the unbroken line in Figure 11, as given in [8].

The length of the stretched zone is denoted by the slip length δ_i. Zone Z will increase, and zone Y will decrease as P is increases. This will continue till $P = P_{\text{amp}}$. Zone Y is then eliminated, and δ_i equals δ_a. The differential equation in this case is the same as when the bar is initially loaded. The only difference is the boundary conditions. Here, the boundary conditions are, as given by [8]:

$$Fdx - EA\frac{d^2u}{d^2x} = 0, \tag{17}$$

$$\begin{aligned} &x = 0, \\ &P = -EA\frac{du_i}{dx}, \qquad x = \delta_i,\ u_i(\delta_a, \delta_i) = u(\delta_a, \delta_i). \end{aligned} \tag{18}$$

Solving (17) with (18) yields u_i at the bar end as a function of δ_a and δ_i:

$$\begin{aligned} u_i(\delta_i, \delta_a) &= \frac{\mu q_0\left(\delta_i{}^2 - \delta_a^2\right)}{2EA}, \\ P_d(\delta_i, \delta_a) &= \mu q_0(2\delta_i - \delta_a), \end{aligned} \tag{19}$$

where δ_i is slip length, when the load is increasing from $-P_{\text{amp}}$ to P_{amp}. The slip length δ_i is calculated by equilibrium of forces for the stretched region Y.

Once the relations of both force and displacement at the end of the bar for both unloading and reloading is established in terms of slip length based on initial loading relationships, the hysteretic curve can be generated. Figure 12 is the time domain representation of input force and Figure 13 is simulated displacement at the end of the bar. Using above parametric functions, the hysteretic curve is established and shown in Figure 14. The curve is built up with a starting part (portion OA) for initial loading, the lower curve (portion AB), for unloading $P_d(\delta_d)$ and $u_d(\delta_d)$, and an upper curve (portion BA) for reloading $P_i(\delta_i)$ and $u_i(\delta_i)$. Once the hysteretic curve is established, the damping energy is calculated. The work done per cycle is

$$W = \oint udP. \tag{20}$$

(5) *Linearization.* The objective here is to transform the nonlinear properties of the friction damper into equivalent linear damping and stiffness. The hysteresis loop made by the force versus displacement function is thereby replaced with an equivalent elliptic loop. The linearized properties of the damper will then be used for forced response analysis. Linearization of the friction model is done by using Lazan's method [9].

The work done by equivalent viscous damping is given by

$$D = \pi\bar{\omega}C_{\text{eq}}u_{\text{amp}}^2, \tag{21}$$

by equating (20) and (21), we get

$$C_{\text{eq}} = \frac{W}{\pi\omega u_{\text{amp}}^2}. \tag{22}$$

Similarly the equivalent stiffness given by Lazan's method is

$$K_{\text{eq}} = \sqrt{\left(\frac{P_{\text{amp}}}{u_{\text{amp}}}\right)^2 - \left(\omega C_{\text{eq}}\right)^2}. \tag{23}$$

2.3. Reduced Model. The dynamically equivalent reduced blade model is represented using a two-degree freedom system simulating 1st flexure mode of blade under investigation, similar to that of given by [8], but additionally the material damping and the aerial damping are represented as a viscous damper. The reason for choosing a two-DOF system for simulations is that it is simple but still illustrates the effect of the damper. At first the response for blade model without damper insert is determined, and correlation is ensured for the first mode between design model and actual blade model. The calculations are performed for various excitation frequency and amplitude of excitation.

The 2-DOF system, shown in Figure 15, is built considering a mass less beam with two concentrated masses simulating aerofoil and the root portions of the blade and damper. The aerial and material damping is considered as a viscous damping and attached to the aerofoil portion of the blade. The friction damper is described by an equivalent viscous damper and spring, $C_{\text{eq}}(\delta_a)$ and $K_{\text{eq}}(\delta_a)$, respectively. Assuming harmonic force of excitation applied at the aerofoil portion of the blade. The displacements where the friction damper is attached and force applied are x_1 and x_2, respectively.

As the model is approximate, for obtaining the quantitative estimations, the model is identified using correction factors based on the statistical results obtained from testing the turbine blade and the modal analysis of a 3D model of the blade. Some of the parameters which are used for correcting the model are as follows.

The value of 1st natural frequency of the blade without a damper insert ($f1$) has provided the values of mass and stiffness of equivalent model.

The damping in the turbine blade without damper insert is in the range of $\zeta \approx 1\%$ as per the statistics provided by experiments and used as a viscous drag in the model.

The value of the excitation force is chosen such that the amplitude of varying stresses in the blade is in the range of 50–100 MPa, this value is estimated from the statistical data available for a typical class of turbine blades.

The friction coefficient is taken in the range of 0.2–0.4 considering the operating environment of the damper inserts.

The equation of motion for the system is

$$\begin{aligned} &M_1\ddot{x_1}(t) + C_{\text{eq}}(\delta_a)\dot{x_1}(t) + \left(K_1 + K_2 + K_{\text{eq}}(\delta_a)\right)x_1(t) \\ &\qquad -K_2x_2(t) = 0, \\ &M_2\ddot{x_2}(t) + C\dot{x_2}(t) + K_2x_2(t) - K_2x_1(t) = P_ae^{j\omega t}. \end{aligned} \tag{24}$$

Assuming harmonic motion:

$$x_1(t) = X_1e^{j\omega t}, \qquad x_2(t)X_2e^{j\omega t}. \tag{25}$$

And defining the complex stiffness

$$K(\delta_a) = K_{\text{eq}}(\delta_a) + j\omega C_{\text{eq}}(\delta_a). \tag{26}$$

By substituting (26) and (25) in (24) yields algebraic equations:

$$-M_1\omega^2X_1 + (K(\delta_a) + K_1 + K_2)X_1 - K_2X_2 = 0, \tag{27}$$

$$-M_2\omega^2X_2 + C\omega X_2 + K_2X_2 - K_2X_1 = P_a. \tag{28}$$

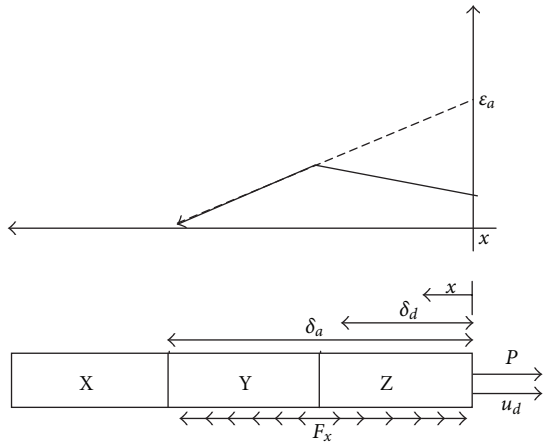

Figure 8: Force, displacement, and plot of strain function, when force is decreasing; zone X is totally struck and has zero strain, zone Y is struck and stretched; zone Z is slipping and compressed.

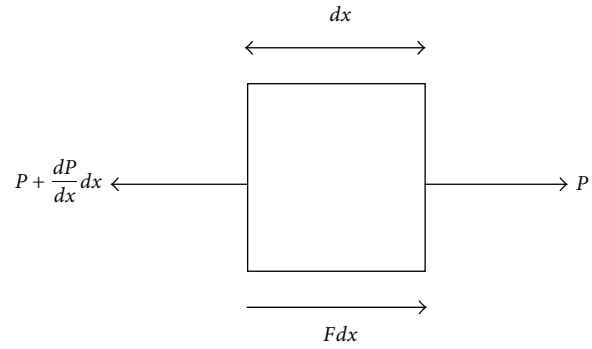

Figure 9: Forces acting on a small element in zone Z, when force is decreasing.

From (28), $X_2 = (P_a + K_2X_1)/(K_2 + jC\omega - M_2\omega^2)$. Substituting X_2 in (27) we get

$$X_1 = \frac{P_aK_2}{(K_2 + jC\omega - M_2\omega^2)\left((K_1 + K_2 + K(\delta_a) - M_1\omega^2) - K_2^2\right)},$$
$$X_1 = \frac{P_a}{(K_2 + jC\omega - M_2\omega^2)} + \frac{P_aK_2^2}{(K_2 + jC\omega - M_2\omega^2)\left((K_1 + K_2 + K(\delta_a) - M_1\omega^2) - K_2^2\right)}. \quad (29)$$

The response of the system is studied keeping the excitation force amplitude constant, and varying the normal load on the damper.

The solution procedure adopted in the frequency-domain is based on finding the response amplitudes iteratively. The excitation level is selected in such a way that the maximum stress in the blade is in the range of 100 MPa. The starting point being the response levels of the underlying linear system. The behaviour of the friction dampers is analyzed at a given relative response amplitude between the damper connection points and the individual dampers. The individual dampers are represented as equivalent complex stiffness, representing both restoring and energy dissipation characteristics as described above. The equivalent complex stiffness is then added to the otherwise linear system, and the response level of the modified system is calculated again. The procedure is repeated till convergence is achieved. The error between successive iterations should be below certain value. In the present case, it is defined as $1E10^{-5}$.

The response levels obtained at current frequency are used as initial guesses for the next frequency increment. Figure 16 shows the normalized responses verses the frequency ratio, under a given excitation for various normalized friction forces. When the friction force is increased the response levels will decrease and attain minimum at particular condition. Further increase in friction force will increase the response amplitude. Figure 17 is the normalized stress versus normalized friction force, and Figure 18 represents plot for damping coefficient verses normalized friction force. The damper design curve/performance curve given in Figure 19, is drawn between normalized response verses normalized excitation, the entire curve can be divided in to three zones, Zone 1 is a completely struck condition. This happens at very low excitation levels or at very high normal loads. In this zone, the system behaves as a linear system. Zone 2 is a slip condition at either low normal loads or at higher excitation level. Here again the system behaves as a linear system. Zone 3 is a slip-stick zone, where the system experiences both conditions in a given cycle, and the system is highly nonlinear in nature.

Figure 20 is the damper performance curve generated for various viscous damping levels. From this figure, it is clear that the damper performance curves depends on the damper properties rather than the normal load and excitation level, which means, for a given damper, one damper performance curve can be generated and that can be used for optimal selection of the damper. These observations are in line with observations made by [2, 3]. The advantage with this representation is that it provides a design point, which is independent of both excitation and viscous damping levels in the engine. The design point is selected corresponding to maximum allowable blade response and consequently, the maximum excitation that can be sustained by the present blade. If actual excitation exceeds this maximum value, then the entire blade must be redesigned since friction damping cannot keep the blade response below allowable limits. Using this approach provides a friction damper that is optimal. The stresses in the blade will be acceptable for as

large an excitation as possible. Thus, the optimal design is independent of the excitation and is insensitive to variations in viscous damping.

3. Experimental Studies

The laboratory experiments were carried out in two phases [16]. The first phase establishes the dynamic characteristics of the blade. This includes estimation of natural frequencies, mode shapes, the logarithmic decrement/damping factors, and the relative stress distribution along the aerofoil for various conditions. The tests are performed for the free-free condition and the clamped condition. In the second phase, the friction damper is characterized. In the present paper, only the relevant and important results are discussed

3.1. Free-Free Condition. In this case, the blade is suspended using a thread and excited using an instrumented impact hammer. The damping estimation by this technique gives only the material damping of the blade (aerial damping due to oscillating blade can be neglected as it is proportionately very small). Knowing this material damping is a must in order to understand the amount of damping blades will experience due to blade fixity in clamped condition.

3.2. Clamped Condition. For this a customized fixture is made in order to accommodate the blade under investigation alongwith the dummy blades on either side with under platform damper inserts. An electrodynamic shaker is used to excite the blade assembly that is driven by the signal generator through the amplifier in the frequency range of interest. The amplitude of excitation is kept constant by using a feedback control loop. The response is measured by blade-mounted strain gages. While placing the strain gauges on the blades, the following aspects are considered:

(1) sensor operability is ensured throughout the operating conditions of the blade;

(2) instrumentation convenience;

(3) informative capability of the strain gauges for the mode of interest.

The first two conditions are usually satisfied by a strain gauge located on blade suction side near aerofoil root. The informative capability of strain gauge is ensured through the 3D FEM analysis and experimental strain survey. One will look for maximum variable stresses for a given oscillation mode. Figure 21 demonstrates the strain gauges pasted on the blade under test. Apart from these strain gages, various other transducers like eddy current probes and accelerometers are used for the rig operation.

The signals measured from strain gages mounted on blade are used for characterizing the blade. When studying frequency characteristics and the damping of fixed blades, it is necessary to identify frequencies using spectral analysis and then finds its attributes, namely, the one caused by blade's resonating frequencies and other caused by excitation of fixture subcomponents. When fixing blades in spring clamps,

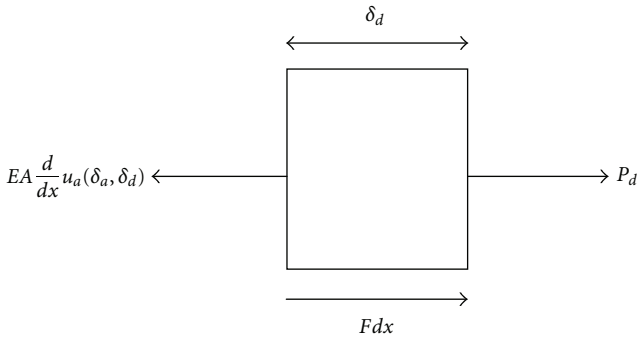

Figure 10: Forces acting on a small element in zone Z, when force is decreasing.

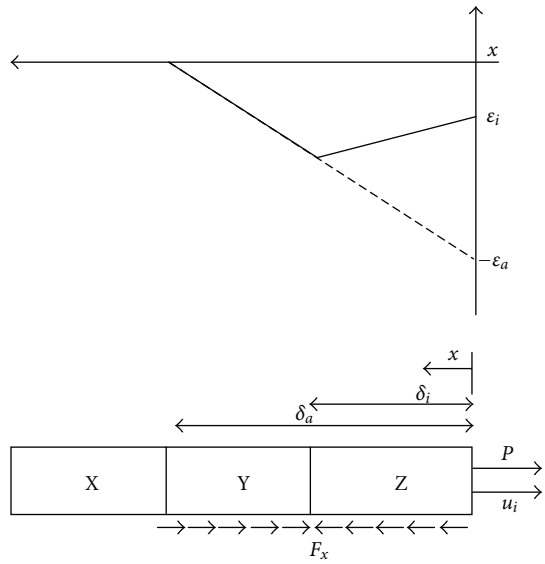

Figure 11: Force, displacement, and plot of strain function, when force is decreasing; zone X is totally struck and has zero strain, zone Y is struck and compressed; zone Z is slipping and stretched.

blade spectrums are investigated for various attachment designs, for different rigidity, mass, and squeezing efforts. Figure 22 shows the single blade setup under clamped condition, while Figure 23 shows the setup for dynamic characterization of blade damper assembly under clamped condition.

Table 3 gives measured natural frequency and corresponding damping value for both the fixity conditions. In both of these tests, it is clear that the first flexure mode is in the range of 1.01f1 and1.03f1. The logarithmic decrement is in the range of 0.5 to 1%, which is within the limits of scatter identified from the free-free test on the individual blade. From the test, it is apparent that the energy dissipation due to friction induced due to the clamping arrangement is very small. Certain divergence in frequency values can be attributed to difference in ways of fixation, scatter of blade geometric features within technological tolerance, and difference of real anisotropy of blade material

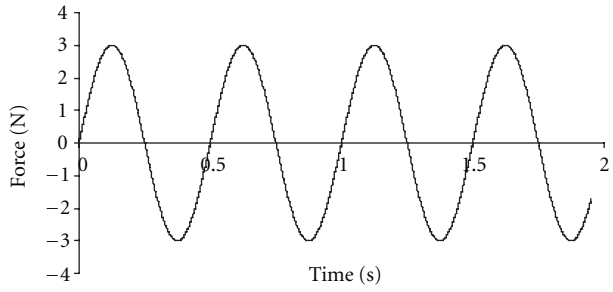

Figure 12: The applied force at the end of the bar.

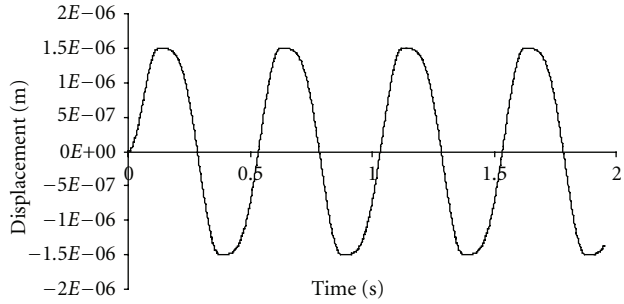

Figure 13: The simulated displacement at the end of the bar.

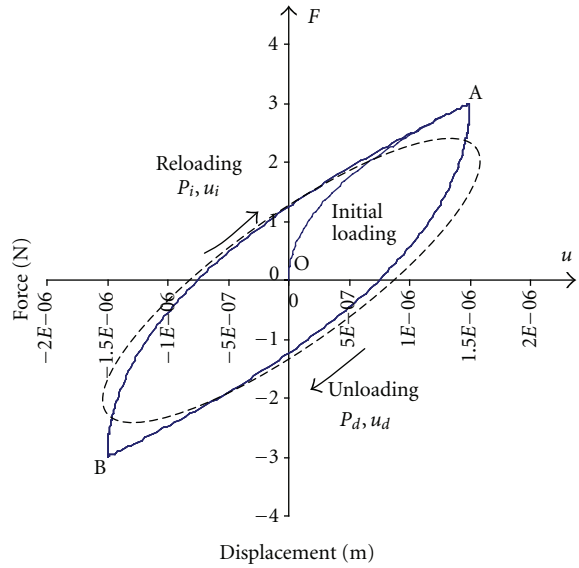

Figure 14: Hysteretic curve drawn between applied force and the simulated displacement at the end of the bar.

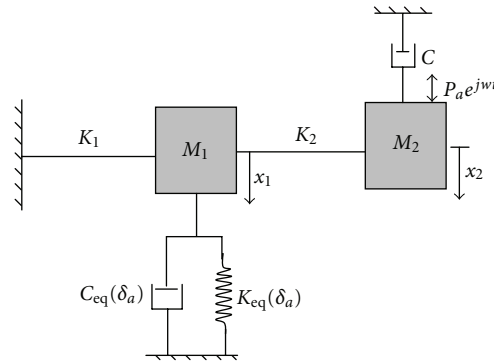

Figure 15: The equivalent blade model, representing two-dof system with friction damper.

from orthotropic parameters set forth in calculations. Tables 4(a) and 4(b) indicate measured values of relative strain corresponding to first flexure mode of the blade under zero normal load on the damper. From the table, it is very clear that the most loaded area on the blade is near root, and the maximum displacement is measured at leading edge, pressure side of the blade. The relative deformation is

$$\overline{\varepsilon_i} = \frac{\varepsilon_i}{\varepsilon_{\max}}, \tag{30}$$

where i is the strain gauge number, $\overline{\varepsilon_i}$ is the relative deformation in blade aerofoil, ε_i is the deformation measured in aerofoil by the ith strain gauge, and $\varepsilon_{\max}$ is the maximum deformation measured by the any strain gauge on blade aerofoil.

3.3. Characterizing Friction Damper. The test setup for this case remains the same as above except for an additional customized feature to load the damper. The test is executed for various conditions of normal loads at controlled excitation level.

The force level is selected such that the maximum stress experienced by the blade is around 100 MPa. The frequency of excitation is selected around the natural frequency of the blade, and the responses were measured till the steady state achieved. The test is repeated for several damper load conditions. The values of resonance frequencies and its logarithmic decrement at different loads of the damper are given in Table 5. It is observed that the highest logarithmic decrement value is 5.08% at 500 N damper load. The natural frequency of the blade increases with increase in damper load, and to a greater extent in case of first bending mode.

Table 3: Measured modal parameters for 1st flexural mode at room temperature.

Blade fixity	Frequency (Hz)	Log decrement %
Spring clamping of root	1.01f1	0.47%
Three blades fixed in a fixture	1.03f1	0.58%

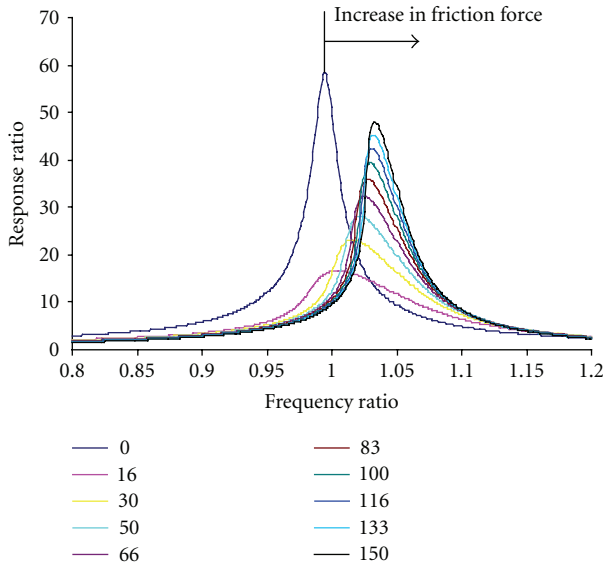

Figure 16: Response ratio versus frequency ratio for various values of normalized friction force.

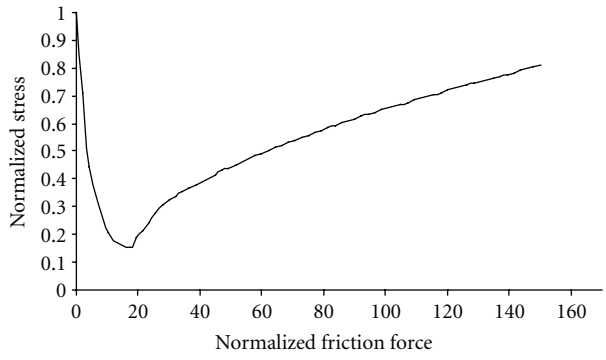

Figure 17: Normalised stress versus normalised friction force.

Table 4: Relative strain at various locations in 1st flexure mode for zero damper load.

(a)

Sl number	1	2	3	4	5	6	7	8
Gauge number	1	2	3	4	1′	2′	3′	4′
Relative strain	1	0.64	0.36	—	0.5	0.42	0.34	0.38

(b)

Sl number	9	10	11	12	13	14	15	16
Gauge number	5′	1′′	2′′	3′′	4′′	I	II	III
Relative strain	—	0.65	0.61	0.36	—	0.15	0.26	0.2

4. Estimation of Damper Efficiency

With the available experimental and theoretical data, the efficiency of the damper insert is evaluated [17].

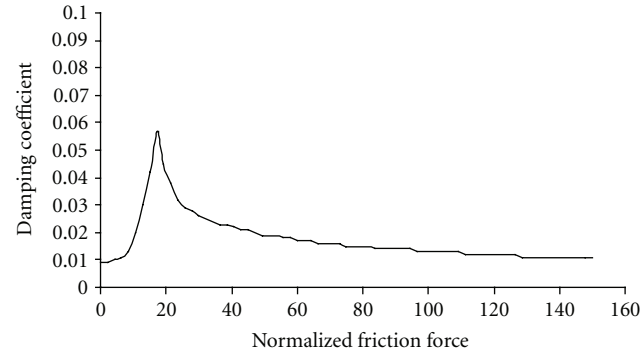

Figure 18: Damping coefficient versus normalized friction force.

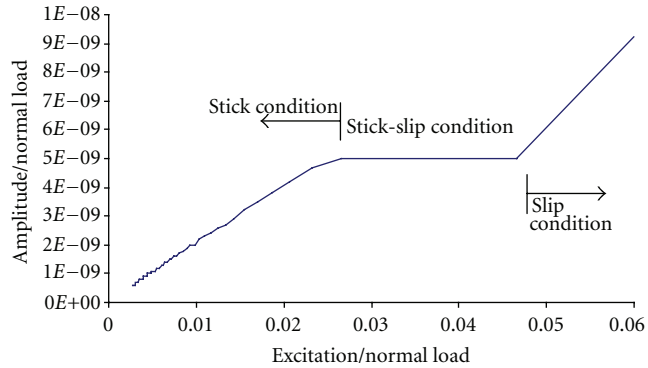

Figure 19: Damper design curve plotted between normalized response and the normalised force.

Table 5: Values of natural frequency and damping of 1st flexure mode of the blade under various damper loads.

Sl number	Damper load (N)	Frequency in Hz	Percentage δ
1	0	1.03f1	0.96
2	300	1.095f1	3.25
3	500	1.154f1	5.08
4	1000	1.170f1	2.54
5	2000	1.191f1	2.5

The normal load generated by the damper at a given operating speed is

$$N = m\omega^2 r,$$
$$m \times r = 1415\,\text{g} - \text{mm}, \tag{31}$$

where m is the mass of the damper in "g", and r is the radius at which damper located in "mm." Angular velocity ω in rads^{-1}.

Figure 24 is a Campbell plot for a blade. It shows two potential resonance conditions corresponding to first flexure mode, due to 6th- and 9th-order cross-overs, at 12000 rpm and 16000 rpm, respectively.

The normal load corresponding to 9th-order cross-over is $N = 1834$ N.

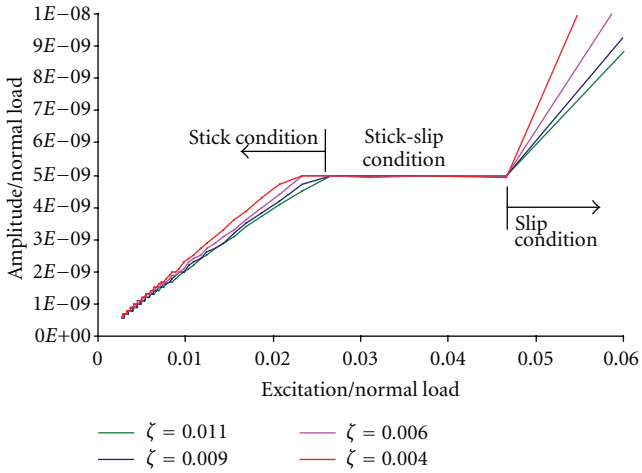

Figure 20: Damper design curve generated under various viscous damping levels.

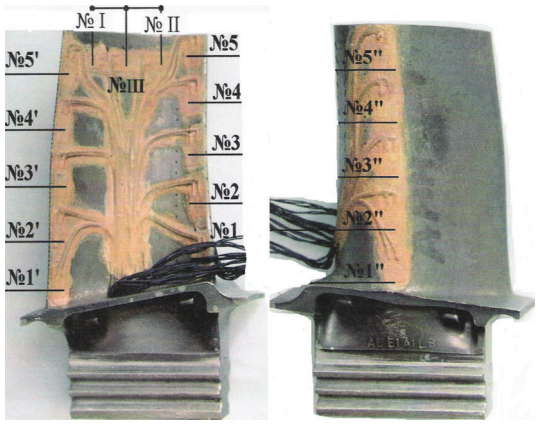

Figure 21: Indicating the strain gauges mounted on both pressure and section side of the blade.

A typical value of friction coefficient for metal-metal contact under slow slide is $\mu = 0.2$. This value under vibrating contact surfaces is known to reduce the contact and the friction ratios. Contrast to this, under high-frequency relative motion of the bodies, frictional seizure phenomena, due to heating of local zones can occur, leading to increase of friction coefficient. Therefore for calculations, a broad range of possible values for μ ranging from 0.2 to 0.4 is considered. The corresponding friction force F for this will be in the range of 180–734 N.

Using various factors generated from the finite element analysis the range of normalized friction force is identified. The ratio of tip displacement to resonant stresses is $k_{u\sigma} = 2.12e^{-3}$ mm^3/N. Considering the resonance stresses in the range of 50–100 Mpa, the displacement of the blade tip is in the range of 0.11 mm–0.2 mm. Once the blade tip displacement is identified using $k_{uP} = 0.026$, the range of excitation P can be identified. Therefore, excitation P is in the range of 4–8 N.

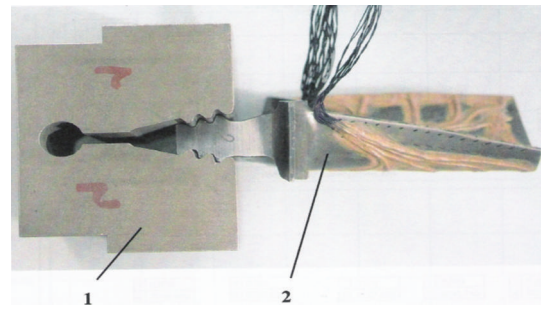

Figure 22: Blade fixation at the root in a spring clamp. (1) spring clamp and (2) blade under investigation.

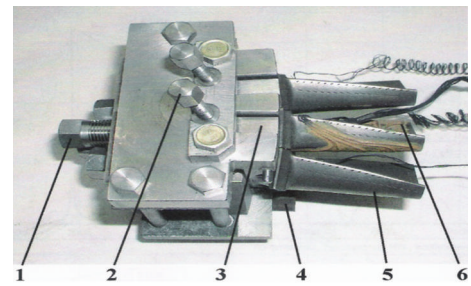

Figure 23: Tooling used for estimation of damper efficiency screw. (2) load screw, (3) lever, (4) support, (5) blade, and (6) strain gauges.

And the range of normalized friction force is calculated as

$$\left(\bar{F}\right)_{\text{cal}} = \frac{F}{P} \text{ is 22 to 174.} \tag{32}$$

Keeping all other parameters constant the $(\bar{F})$ is normalized friction force, proportional to the normal load applied on the damper.

Therefore, $(\bar{F})/N = \text{cont}'$.

The optimum range of normalized friction force corresponding to maximum rotational frequency can be found from

$$\left(\bar{F}\right)_{\text{opt}} = \frac{N_{\text{opt}}}{N}\left(\bar{F}\right)_{\text{cal}}, \tag{33}$$

where N_{opt} is the optimum damper load at which the response of the blade is minimum, that is, 500 N, and N is the normal load on the damper at a given rotational speed.

Therefore, the $(\bar{F})_{\text{opt}}$ is in the range of 6 to 47. In this range of friction forces significant reduction in stresses is expected. Further increase in normal load may increase the aerofoil stresses.

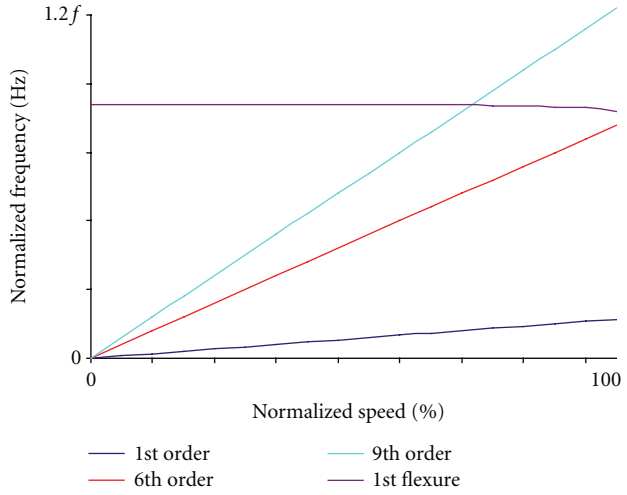

Figure 24: Campbell diagram, indicating 1st flexure mode with various excitation lines.

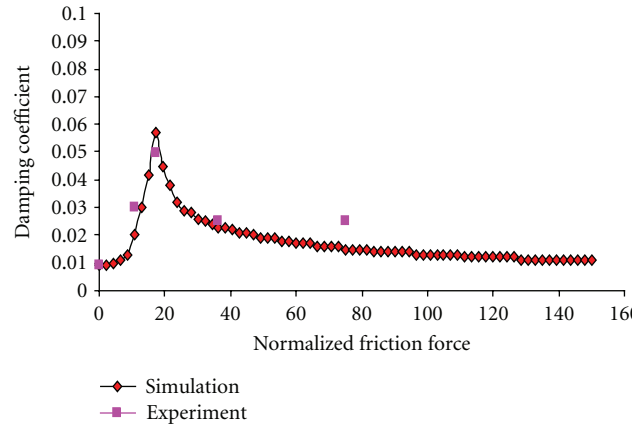

Figure 25: Comparison of damping coefficient value with normalized friction force.

5. Comparison of Analytical and Experimental Findings

The correlation studies is carried out in two phases, in phase one, the dynamic characteristics of the blade under investigation is carried out, which includes the natural frequency, mode shape, and the damping. Further it is ensured that the blade fixity will have negligible effect on the damping. The relative strain estimated along the aerofoil for the first flexure mode is in good correlation with experiments conducted without damper inserts. The damper effectiveness is measured on bench test is in good agreement with the analytical findings. The maximum logarithmic decrement value measured with damper insert is around 5.08%, in case of analytical estimation it is around 5.8%. From the experiments it is found that the optimal normalized friction force is in the range of 6–47, for the blade damper system under investigation, corresponding to the rotational speed of 16000 rpm, where the possibility of 1st flexure mode resonance exists. Similarly in the analytical solution, it is found to be in the range of 7–50, refer to Figure 16. It is clear that the range of normalized friction force for which the response amplitude is below 50% of resonance amplitude without a damper insert. Figure 25 indicates the comparison of both theoretically estimated and the experimentally measured damping coefficient.

6. Conclusions

Minimization of resonant stresses in turbine blades is a major concern in turbine engine. A detailed procedure is outlined for optimization of damper for turbine blade so that the maximum stress experienced by any blade should be below some designated maximum value. The procedure details the integration of analytical and experimental studies to ensure the correctness of the model developed and the friction damper design. A damper performance curve is established, which provides a design point that is independent of both damping and the excitation levels, these two quantities are very difficult to be determined for the new design of blades. At the same time, the design point optimizes the friction damper for as large an excitation as possible. A unique test fixture is developed for conducting the experiments, having a feature to setup various damper loads.

The predicted natural frequencies, stress distribution, and the displacements determined for the 1st flexure mode of the blade is in good correlation with the experimental results. The damper performance curves are generated for various levels of force and the damping values, which are used to arrive at optimal damper design. This can now be extended to the engine condition, namely, gas loads, and temperatures.

Nomenclature

F_x:	Friction force
μ:	Friction coefficient
δ_a:	Maximum slip corresponding to P_{amp} in "m"
u:	Displacement at the end of the bar in "m"
P:	Excitation at the end of the bar in "N"
N:	Total normal load acting on the interface in "N"
$q(x)$:	Normal load function
L:	Length of the bar = 0.02 "m"
EA:	Modulus of elasticity multiplied with area = 600000 "N"
$\bar{\omega}$:	Angular velocity rads^{-1}
P_{amp}:	Maximum value of the force "N"
u_{amp}:	Maximum displacement "m"
$P_a(\delta_a)$:	Force at the end of the bar corresponding to the initial loading

$u_a(\delta_a)$:	Displacement at the end of the bar corresponding to the initial loading
$P_d(\delta_a, \delta_d)$ and $u_d(\delta_a, \delta_d)$:	Force and displacement at the end of the bar for unloading
$P_i(\delta_a, \delta_i)$ and $u_i(\delta_a, \delta_i)$:	Force and displacement at the end of the bar for reloading
D:	Equivalent damping energy
C_{equ}:	Equivalent viscous damping in "Nsm^{-1}"
W:	Work done per cycle
K_{equ}:	Equivalent stiffness "Nsm^{-1}"
C:	Viscous damping coefficient Nsm^{-1}
dx:	Elemental length of the bar
du/dx:	Strain in the bar
δ:	Slip in the bar in "m".

Acknowledgment

The authors would like to thank the Director of GTRE, for his support throughout this work. And authors also would like to thank the Head of Mechanical Engineering Department, SV University, for his encouragement and guidance and Mr. Sreelal Sreedhar, Additional Director, GTRE, for his valuable inputs. Finally authors thank one and all whomever directly and indirectly involved and helped during this work.

References

[1] J. H. Griffin, "A review of friction damping of turbine blade vibration," *International Journal of Turbo and Jet Engines*, vol. 7, pp. 297–307, 1990.

[2] T. M. Cameron, J. H. Griffin, R. E. Kilb, and T. M. Hoosac, "An integrated approach for friction damper design," *The Role of Damping in Vibration and Noise Control*, vol. 5, pp. 205–211, ASME Booklet DE, 1987.

[3] R. Kilb, J. Griffin, and C. H. Menq, "Evaluation of a turbine blade damper using an integral approach," in *Proceedings of the 29th Structures, Structural Dynamics and Materials Conference AIAA/ASME/ASCE/AHS*, no. 88-2400, AIAA, Williamsburg, Va, USA, 1998.

[4] K. Y. Sanliturk, D. J. Ewins, R. Elliott, and J. S. Green, "Friction damper optimization: simulation of rainbow tests," *Journal of Engineering for Gas Turbines and Power*, vol. 123, no. 4, pp. 930–939, 2001.

[5] C. H. Menq, J. H. Griffin, and J. Bielak, "Influence of a variable normal load on the forced vibration of a frictionally damped structure," *Journal of Engineering for Gas Turbines and Power*, vol. 108, no. 2, pp. 300–305, 1986.

[6] C. H. Menq, J. Bielak, and J. H. Griffin, "The influence of microslip on vibratory response, part I: a new microslip model," *Journal of Sound and Vibration*, vol. 107, no. 2, pp. 279–293, 1986.

[7] C. H. Menq, J. Bielak, and J. H. Griffin, "The influence of microslip on vibratory response, Part II: a comparison with experimental results," *Journal of Sound and Vibration*, vol. 107, no. 2, pp. 295–307, 1986.

[8] G. Csaba, *Modelling microslip friction damping and its influence on turbine blade vibrations*, Dissertations no. 519, Linköping, Sweden, 1998.

[9] G. Csaba, "Forced response analysis in time and frequency domains of a tuned bladed disk with friction dampers," *Journal of Sound and Vibration*, vol. 214, no. 3, pp. 395–412, 1998.

[10] E. Cigeroglu and H. N. Ozguven, "Nonlinear vibration analysis of bladed disks with dry friction dampers," *Journal of Sound and Vibration*, vol. 295, no. 3–5, pp. 1028–1043, 2006.

[11] C. W. Schwingshackl et al., "Measured and estimated friction interface parameters in a nonlinear dynamic analysis," *Mechanical Systems and Signal Processing*, vol. 28, pp. 574–584, 2012.

[12] E. P. Petrov and D. J. Ewins, "Advanced modeling of underplatform friction dampers for analysis of bladed disk vibration," *Journal of Turbomachinery*, vol. 129, no. 1, pp. 143–150, 2007.

[13] J. Szwedowicz, C. Gibert, T. P. Sommer, and R. Kellerer, "Numerical and experimental damping assessment of a thin-walled friction damper in the rotating setup with high pressure turbine blades," *Journal of Engineering for Gas Turbines and Power*, vol. 130, no. 1, Article ID 012502, 2008.

[14] M. Allara, "A model for the characterization of friction contacts in turbine blades," *Journal of Sound and Vibration*, vol. 320, no. 3, pp. 527–544, 2009.

[15] C. M. Firrone, S. Zucca, and M. M. Gola, "The effect of under platform dampers on the forced response of bladed disks by a coupled static/dynamic harmonic balance method," *International Journal of Non-Linear Mechanics*, vol. 46, no. 2, 2011.

[16] Vibration Engineering Group, "Experimental investigation on turbine blade damper," Internal Report, GTRE, Bangalore, India.

[17] Vibration Engineering Group, "Turbine blade damper optimization studies," Internal Document, GTRE, Bangalore, India.